Demonstration of Guided Wave Sensor Signals Effected by Cyclic Loads and Breathing Fatigue Cracks

M. VOSPERNIG, R. HEUER and M. REITERER

ABSTRACT

This paper presents an examination of ultrasonic guided waves (UGW) affected by stress in the wave-guide. Detecting faults in structures with sparse sensor arrays are widely established. The environmental influence of the sensor signals are significant and have to be compensated when baseline concepts are used in the sense of structural health monitoring. This investigation demonstrates, based on experimental observations, deviations of sensor signals caused by a tensioned or compressed wave-guide. To evaluate the behavior of the signal deviations a numerical model is developed. Taking stress-stiffening into account, the change of the sensor signals results from the deviation of the propagation characteristics. Although the wave characteristics are multimodal, one mode, namely the flexural A0 mode, is extracted and the signal deviations are reduced in the space domain. This is performed by a dispersion compensation process and the adaption of the dispersion curves to the stiffness of the wave guide. The procedure is applied to the numerical and the experimental signals and the improvement in the accuracy of the residual signals is presented.

INTRODUCTION

Civil infrastructure owners are interested in monitoring their structures when they are exposed to extraordinary loads or structural changes are applied. The implementation of Structural Health Monitoring (SHM) systems during the

Michael Vospernig, RED Bernard GmbH, Nordbahnstr. 36, 1020 Vienna, Austria
Rudolf Heuer, Vienna University of Technology, Center of Mechanics and Structural Dynamics, 1040 Vienna, Karlsplatz 13/E2063, AUSTRIA
Michael Reiterer, RED Bernard GmbH, Nordbahnstr. 36/Top 2.7, 1020 Vienna, Austria

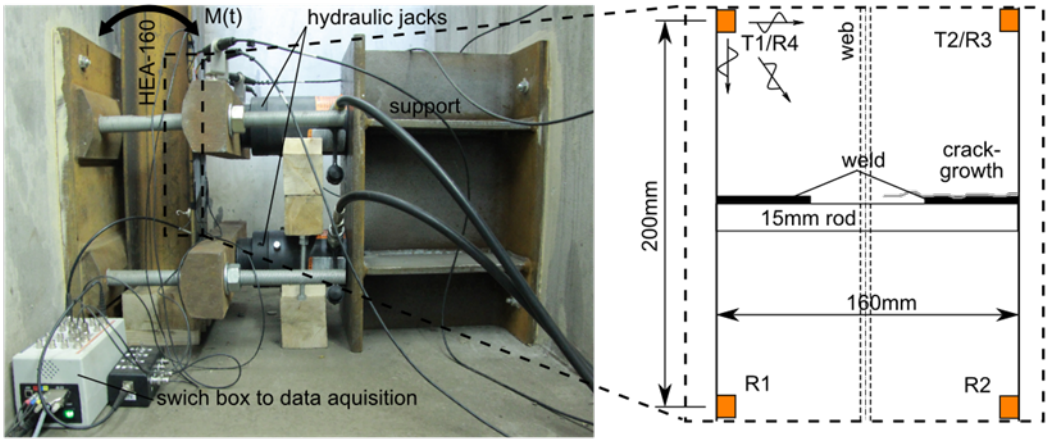

Figure 1. Experimental setup of the fatigue test with a detail of the guided ultrasonic sparse array.

manufacturing process is increasing because owners are interested in recording data for a later "condition assessment" [1]. Because the life time of a civil structure is expected to be 50 years and more , it is challenging to provide comparable data from the first to the last day of the recording. To assure a long-time stability of precise measuring, operational effects have to be taken into account and well documented. Environmental effects resulting from temperature [2, 3, 4], loads [5] or humidity are in the focus of the scientific community in the field of guided wave SHM. This is addressed to the SHM axiom of comparing between two different system states to extract a feature from the sensor signals [6] to evaluate the change of a system. The investigation of operational effects is related to the SHM system. It is highlighted how sensitive guided waves are to stress in the observed structure. This stress can lead from external forces or temperature restraints. Effects on the sensor itself or the measuring hardware are not investigated.

This paper is dived in 3 chapters. First, signal deviations of a sparse guided wave array applied to a vibrating I-beam experiment are presented [7]. Second a numerical model is developed to evaluate the effected of signal deviation caused by a tensioned or compressed wave-guide. And third, compensation is introduced by an application of the dispersion compensation algorithm with an adaption of the dispersion curves to the wave-guide stiffness.

EXPERIMENTAL STUDY

The presented experiment of this section is extensively documented in [7] and is used to evaluate the considerations of the sections above. A fatigue test was carried out on a HE-A 160 cantilever I-beam with a total height of 3m. The specimen was clamped in an upright position with hydraulic jacks and mass was added on top of the cantilever. Exciting the beam at its eigen-frequency caused a harmonic vibration of the system and a bending moment at the clamped support. A rod with a diameter of 15mm was welded on one flange in the proximity of the support to provoke a stress concentration. In combination with the cyclic loading, this notch leads to a fatigue hot spot where cracks occurred. A detail of the fatigue zone is illustrated in Figure 1. A displacement transducer on top of the beam

controlled the process and the maximal defection was kept constant (e.g. ±12mm). Hence the stress range at the fatigue zone was constant too (e.g. ±80MPa). The end of the test was achieved when a crack appeared and its size influenced the response of the vibrating cantilever in a way that the defection declined.

The sensor array was applied to the flange of the beam as demonstrated in figure 9. In this application the wave-guide was the plate like 9mm flange of the I-beam, whereas 3 propagation paths were recorded when a transmitter was excited. The actuation and data acquisition were carried out by the commercial SHM system USPC 5000 [8] to record the system state signals $s_{ik}(t)$. To maximize the wave response by exciting the 10x10mm PZT-elements, frequency adjustments were performed with mode tuning [9]. For an A0 excitation of the 9mm flange, 166kHz was the adapted frequency. The burst form was a 2.5 cycle box windowed sinus because the analogue signal generator of the USPC 5000 does not support other window functions. While the cantilever beam was harmonically vibrating with 9.2Hz every 5 minutes an ultrasonic burst was transmitted and the signals were recorded by the sensor array.

Observed operational effects

Exemplarily the sensor path signals $s_{1k}(t)$ from T1 to R1 are taken into account to illustrate the influence of the stressed wave guide. The vibration of the beam causes a tension and compression of flange when the waves are transmitted. The condition of the flange when a burst is sent every 5 minutes can be evaluated implicit. The flexural stress distribution of the I-beam is approved to be constant across the thickness of the wave-guide and along the path. An influence of temperature was excluded because the structure temperature was observed and remained constant.

Sequences of the normalized signals for the undamaged beam are presented in Figure 2. It illustrates a clear clustering of the signals at different system states. When no fault is present it is assumed that a tension of the wave-guide leads to faster wave velocities and vice versa when the wave guide is compressed. Moreover the normalization of the first wave pack point out an amplitude damping

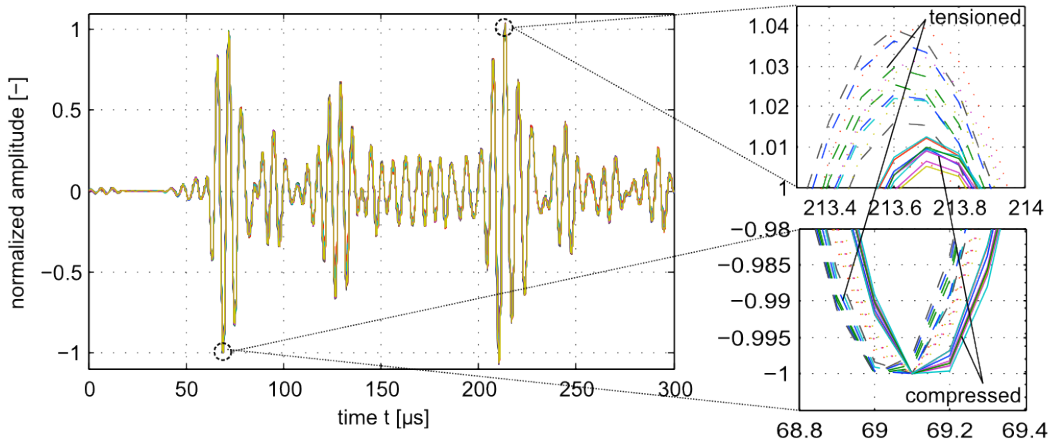

Figure 2. Comparison of 30 recorded sensor signals $s_{1k}(t)$ when the beam is vibrating and no fault is present. The signal deviations are addressed to the tensioned or compressed wave guide.

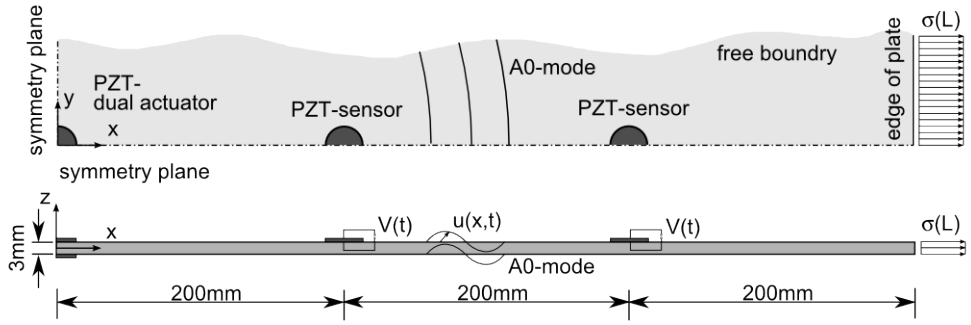

Figure 3. FE plane strain model of a 3mm wave guide with one dual PZT-element actuator and 2 single PZT-element sensors.

for the compressed system state as illustrated in the detail of Figure 2 for a later arriving wave pack. To determine these assumptions a numerical model is introduced.

NUMERICAL VALIDATION

As described earlier the influence of the tensioned or compressed wave guide on the sensor signals was observed. The different system states of the structure cause stress-stiffening, a change in the thickness and a change in the distance between transmitter and receiver. Hence it is not well-defined which system state leads to positive or negative time shifts.

For this investigation a plain strain multi-physics finite element (FE) model according to Figure 3 with the propagation of straight crested waves was accomplished. A 3mm thick structural steel (S235) plate was modeled with a dual PZT-element actuator (PIC255) and two sensors in the distance of 200mm and 400mm from the actuator. The bonding of the PZT-elements was assumed to be perfect and no material damping was taken into account. The boundary conditions for the PZT-elements were electrical fields across the thickness. For the excitation, a 5 cycle 65 kHz Hanning windowed tone burst was applied with a peak to peak amplitude of 100V. To provoke time shifts δt the plate was pre-stressed with a constant stress distribution $\sigma(L)$ at the end of the plate. For the space resolution, regarding to the excited A0 wave mode, 1mm was the global element size and

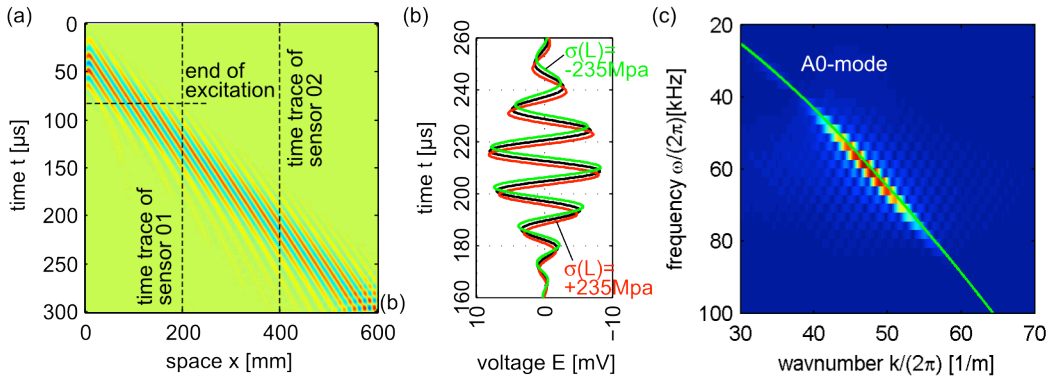

Figure 4. FE results (a) surface deformation $u_z(x,t)$, (b) comparison of the sensor 2 signals $s_{ik}(t)$ for the 3 system states of the wave guide, and (c) 2D FFT of the $u_z(x,t)$ to determine the wave-numbers compared with the results from the Rayleigh-Lamb frequency equation (green line).

approximately 0.1mm in the proximity of the PZT-elements. The time step was $0.1\mu s$ to guarantee small signal phase shifts due to the mechanical stress. Three calculation were performed, one without stress, one with $\sigma(L) = +235MPa$ tension and one with $\sigma(L) = -235MPa$ compression. The results of the out of plane surface deformations $u_z(x, z = +d/2;t)$ and the sensor signal $s_{ik}(t)$ were used for further interpretation and are exemplarily illustrated in Figure 4. Figure 4b clearly illustrates the stress-stiffening effect of the wave-guide. It points out that in case of the tensioned wave-guide the phases arrive earlier, although the path of propagation is extended. However the phases arrive delayed, for the compressed wave-guide.

Determination of the time shifts

A straight forward approach to compare signals is the cross-correlation. This is acceptable because the sensor results represent only the wave pack travelled from the actuator to the sensor and the spatial spread of the PZT-element is neglected. Consequently the time shifts are approximately constant for the computed sensor signal. The cross-correlation function is given as

$$\Psi_{ik}(\tau) = \lim_{T\to\infty} \frac{1}{T} \int_0^T s_{i0}(t)\, s_{ik}(t+\tau)\, dt \tag{1}$$

and the time shift δt is expressed by

$$\delta t = \arg\max(\Psi_{i0}) - \arg\max(\Psi_{ik}), \tag{2}$$

where Ψ_{i0} is the auto-correlation of the non pre-stressed signal $s_{i0}(t)$. The time shift results are summarized in Figure 5 where a clear linear increase of the time shift with increasing sensor distance is described.

In the second approach the surface deformations $u_z(x\ t)$ as illustrated in Figure 4a are adopted to compute the wavenumbers and the deviations according to the stress distribution. To obtain the spectral information of the frequency and wavenumber domain of the array in Figure 4a, a Fourier transform in time (column) and the spacial (row) domain is applied [10]. The expression for the 2D Fourier transform is given by

$$U_z(k,\omega) = \int_{-\infty}^{\infty}\int_{-\infty}^{\infty} u_z(x,t)\, e^{-i(kx-\omega t)}\, dx\, dt\,. \tag{3}$$

Because the FE results are available in discrete form, the 2D-FFT algorithm was applied. As a result an array of the frequency and wavenumber content will be obtained. An image of an executed transformation is presented in Figure 4c for the stress-free wave-guide. Additionally the wavenumber solution of Rayleigh-Lamb frequency equation [11] is displayed to approve sufficient accuracy of the FE-model.

The results of the two methods are summarized in Figure 5. Physically is concluded, that times shifts increase proportional with the distance of the propagating wave. This is illustrated in Figure 5a. The deviation of the wavenumer is not proportional to the frequency nor the wavenumber, which is illustrated in Figure 5b. If only a change in the material stiffness would be present, then the frequency $\omega_i(k)$ of the system state i are given by a coefficient

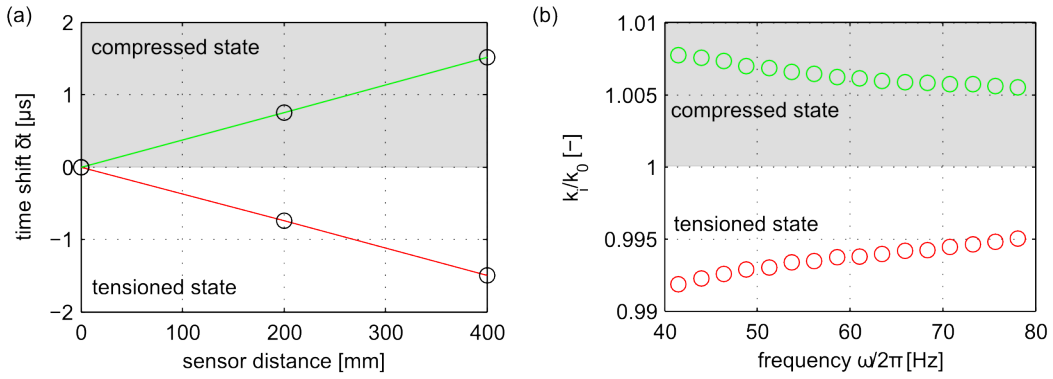

Figure 5. Determination of time shifts of the FE simulations. (a) Cross-correlation results of the sensor signals and (b) results from the 2D-FFT wavenumber deviations.

$$\omega_i(k) = \omega_0(k)\sqrt{E_i/E_0} \tag{4}$$

where E_i is the Modulus of elasticity for a isotropic material. Because the results of Figure 5b are not linear it is assumed, that the deviation regard to multiple parameters.

COMPENSATION IN THE SPACE DOMAIN

For a later localization of a crack the time signals are transformed in the space domain. Because of the presents of only one wave mode the author uses the dispersion compensation (DC) algorithm [12].

$$s_{1k}(t) \xrightarrow{FFT} F_{1k}(\omega) \xrightarrow{DC} G_{1k}(k) \xrightarrow{IFFT} g_{1k}(x) \tag{5}$$

The approach to compensate the time shifts is done by a manipulation of the dispersion curves used in the DC algorithm. Two parameters are used to manipulate the dispersion curves. As illustrated in Figure 6, the initial dispersion curves k_0 are numerical computed in the wavenumber domain k with the according frequencies $\omega(k)$. Frequency shifts are applied by a coefficient of stiffness of Equation 4 and

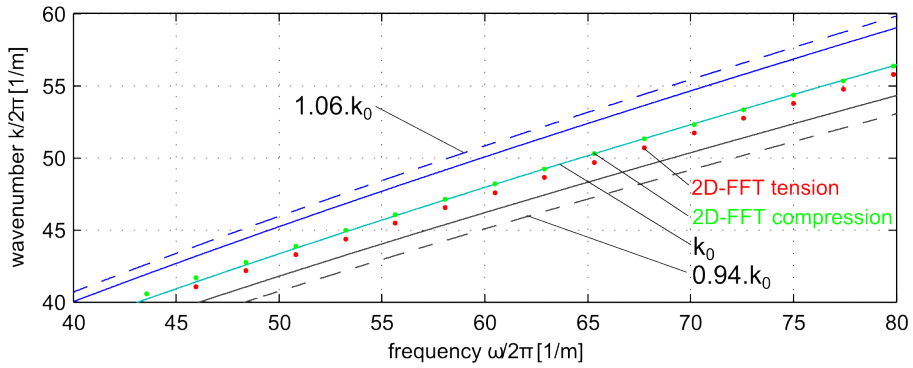

Figure 6. Manipulation of the dispersion curves for the DC algorithm. A0 mode, structural steel (E=210GPa, ν=0.2, 3mm plate thickness.

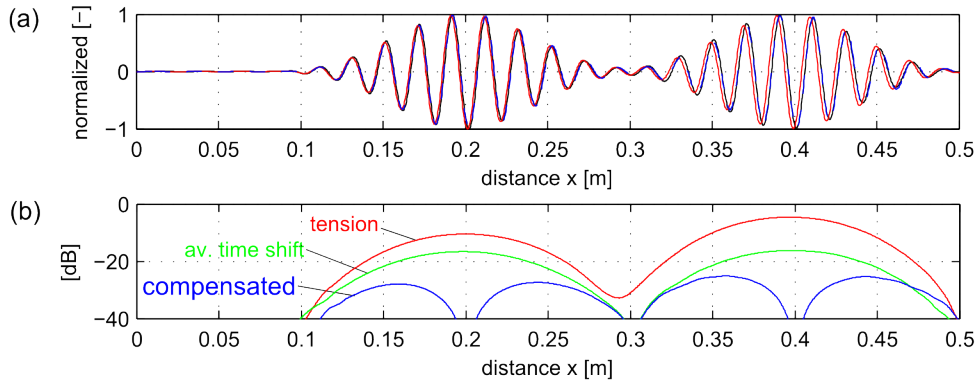

Figure 7. Results from the compensated FE-simulated signals. (a) added and normalized sensor signals and (b) signal deviations of the pre-stressed and unstressed wave guide.

wavenumber shift are realized by a variation of the thickness of the wave guide. The best compensation results are achieved by liner shifts in the wave number domain.

Finally the compensation is applied to the signals from the numerical simulation. The signals of the two sensors are added to characterize multiple wave packs in one signal propagating different distances. A determination of the improvement of the compensation is presented in Figure 7. In Figure 7a the phase shifts between the black $g_0(x)$ and the red line $g_i(x)$ is clear, especially for the second wave pack. The differences of the residual signals in Figure 7b are expressed by

$$R_i(x) = 20\log_{10}\left(\mathrm{H}\left\{g_0(x) - g_i(x)\right\}\right) \tag{6}$$

where H is the operator of the Hilbert transform to calculate the envelop of the residual signal. The red line represents the residual with no compensation and the blue the residual of the compensated signal. The improvement is distinct for both wave packs, whereas the best match is concentrated around the exact sensor locations. Remaining inaccuracy regards to a deviation of the amplitudes. Amplitude deviations are not compensated and are more distinct then in the numerical simulation.

The compensation algorithm was applied to the signals of Figure 2. The signal match shows the same results and improvements as the numerical investigations. Significant is that the deviation are not completely eliminated but are clearly reduced. This results in better accuracy in the feature detection when a crack occurs.

CONCLUSIONS

A method is presented to compensate time shifts between ultrasonic guide wave signals recorded at different system states. The compensation shows good results when the actuation of one wave mode is assumed and the application was adapted to a stressed waveguide. To compensate the time shifts, dispersion curves are manipulated and the time shift is compensated in the space domain. It is evident,

that very little deviations of the wave numbers, provoked by environmental effects lead to significant deviations in the time domain. Uncompensated residual signals lead to uncertainties in the feature detection for a SHM application. The compensated residual signals are more accurate and the feature is clear when a threshold feature is defined.

Concluding from the presented results the algorithm is capable of development. A two parameter (thickness and stiffness of the wave guide) approach has to be developed to optimize the dispersion curve manipulation and the numerical implementation is focused on a fast algorithm. Finally it is assumed that the compensation is also applicable of environmental effects as temperature.

REFERENCES

1. Brownjohn, J. 2007."Structural Health Monitoring of civil Infrastructure:" *Philosophical Transactions of the Royal Society A*. 365: 589-622.
2. Croxford, A., P. Wilcox, B. Drinkwater, G. Konstantinidis 2007. "Strategies for guided-wave structural health monitoring". *Poc. R. Soc. A* 463, 2961–2981.
3. Clarke, T. 2009. *Guided wave health monitoring of complex structures.* Ph. D. thesis, Imperial College London.
4. Roy, S., K. Lonkar, V. Janapati, F. Chang 2011. "Physics based temperature compensation strategy for structural health monitoring." *In Proc. of the 8th IWSHM*, pp. 1139–1149.
5. Michaels, J., S. Lee, X. Chen, T. Michaels 2011. "Load-enhanced imaging of fatigue cracks via sparse guided wave arrays." *In Proc. of the 8th IWSHM,* pp. 1150–1157.
6. Worden, K., C. Farrar, G. Manson, G. Park 2007. "The fundamental axioms of structural health monitoring." *Phil. Trans. Roy. Soc. A* 463, 1639–1664.
7. Vospernig, M., R. Heuer, & M. Reiterer 2011. "Fatigue crack monitoring with an ultrasonic sparse array on a real steel structure component." *In Proc. of the 8th IWSHM*, pp. 669–676.
8. Hillger, W. 2006. *Manual of the USPC 5000. Technical report*. Ingenieurbüro Dr. W. Hillger.
9. Giurgiutiu, V. 2005. "Tuned lamb wave excitation and detection with piezoelectric waver active sensors for structural health monitoring." *J. Intelligent Materials Systems and Structures* 16, 291–305.
10. Alleyne, D. P. Cawley 1991. "A two-dimensional Fourier-transform method for the measurement of propagating multimode signals." *J. Acoust. Soc. Am.* 89, 1159–1167.
11. Rose, J. L. 1999. *Ultrasonic Waves in Solid Media*. Cambridge University Press.
12. Wilcox, P. 2003. "A rapid signal processing technique to remove the effect of dispersion from guided wave signals." *IEEE Transactions on Ultrasonics, Ferroelectrics and Frequency Control* 50(4), 419–427.